18F-FDG-PET/MR increases diagnostic confidence in detection of bone metastases compared with 18F-FDG-PET/CT

Samarin, Andrei ; Hüllner, Martin ; Queiroz, Marcelo A ; Stolzmann, Paul ; Burger, Irene A ; von Schulthess, Gustav ; Veit-Haibach, Patrick

Abstract: PURPOSE: The aim of this study was to compare detection, lesion conspicuity and reader confidence of F-fluorodeoxyglucose (F-FDG)-PET/MR and F-FDG-PET/computed tomography (CT) in patients with F-FDG avid bone metastases. MATERIALS AND METHODS: In this prospective study, a total of 30 PET/CT and PET/MRI data sets were performed in 24 patients. Each examination was evaluated for the presence of PET-positive bone lesions consistent with metastatic involvement. Conspicuity of PET-positive bone lesions was evaluated on the corresponding PET/CT and PET/MR images and compared using the Wilcoxon signed-ranks test. Reader confidence was determined to evaluate whether PET/CT or PET/MR was more useful for the assessment of the bone metastases and was compared using Student's t-test. RESULTS: Overall, in both examinations, PET/CT and PET/MRI detected 86 F-FDG-positive bone lesions. On all 30 PET/MRI examinations, at least one morphological correlate for F-FDG-positive bone lesions was found on the MR component (82 out of 86 lesions). PET/CT imaging allowed identification of corresponding structural changes on the CT component in 23 out of 30 studies (65 out of 86 lesions). In lesion-by-lesion analysis, the mean lesion conspicuity was significantly better on T1 fat MR imaging compared with CT imaging (P=0.005). In seven out of 30 studies, a significant increase in reader confidence of PET/MRI compared with PET/CT was found. CONCLUSION: PET/MRI offers higher reader confidence and improved conspicuity in bone metastases compared with PET/CT. However, the overall detection rate was not different. The highest possible clinical impact of PET/MRI appears to be in patients with limited, early bone metastatic disease.

DOI: https://doi.org/10.1097/MNM.0000000000000387

Original article

Nuclear Medicine Communications

^{18}F-FDG-PET/MR increases diagnostic confidence in detection of bone metastases compared with ^{18}F-FDG-PET/CT

Andrei Samarin[a,e], Martin Hüllner[a,c,d], Marcelo A. Queiroz[a], Paul Stolzmann[a,b,d], Irene A. Burger[a,b,d], Gustav von Schulthess[a] and Patrick Veit-Haibach[a,b,d]

Purpose **The aim of this study was to compare detection, lesion conspicuity and reader confidence of ^{18}F-fluorodeoxyglucose (^{18}F-FDG)-PET/MR and ^{18}F-FDG-PET/computed tomography (CT) in patients with ^{18}F-FDG avid bone metastases.**

Materials and methods **In this prospective study, a total of 30 PET/CT and PET/MRI data sets were performed in 24 patients. Each examination was evaluated for the presence of PET-positive bone lesions consistent with metastatic involvement. Conspicuity of PET-positive bone lesions was evaluated on the corresponding PET/CT and PET/MR images and compared using the Wilcoxon signed-ranks test. Reader confidence was determined to evaluate whether PET/CT or PET/MR was more useful for the assessment of the bone metastases and was compared using Student's *t*-test.**

Results **Overall, in both examinations, PET/CT and PET/MRI detected 86 ^{18}F-FDG-positive bone lesions. On all 30 PET/MRI examinations, at least one morphological correlate for ^{18}F-FDG-positive bone lesions was found on the MR component (82 out of 86 lesions). PET/CT imaging allowed identification of corresponding structural changes on the CT component in 23 out of 30 studies (65 out of 86 lesions). In lesion-by-lesion analysis, the mean lesion conspicuity was significantly better on T1 fat MR imaging compared with CT imaging ($P = 0.005$). In seven out of 30 studies, a significant increase in reader confidence of PET/MRI compared with PET/CT was found.**

Conclusion **PET/MRI offers higher reader confidence and improved conspicuity in bone metastases compared with PET/CT. However, the overall detection rate was not different. The highest possible clinical impact of PET/MRI appears to be in patients with limited, early bone metastatic disease.** *Nucl Med Commun* **00:000–000**

Nuclear Medicine Communications 2015, **00**:000–000

Keywords: bone metastases, hybrid imaging, PET/CT, PET/MR

Departments of [a]Nuclear Medicine, [b]Diagnostic and Interventional Radiology, [c]Department of Neuroradiology, University Hospital Zurich, University of Zurich, [d]University of Zurich, Zurich, Switzerland and [e]Department of Medical Radiology, North Estonia Medical Centre, Tallinn, Estonia

Correspondence to Andrei Samarin, MD, Department of Medical Radiology, North Estonia Medical Centre, Sutiste tee 19, 13419 Tallinn, Estonia
Tel: +372 6171147; fax: +372 6171242; e-mail: andsam@gmail.com

Received 3 April 2015 **Revised** 1 August 2015 **Accepted** 20 August 2015

Introduction

The presence of bone metastases is a major prognostic factor in patients with oncological disease. Early and confident detection of bone metastases enables accurate staging and selection of the optimum treatment of oncological disease.

Multiple imaging techniques are currently available for the detection of the metastatic bone disease including bone scintigraphy, CT, MR and PET/CT imaging [1,2]. Recently, PET/MR hybrid imaging was introduced as a promising tool in oncological imaging research [3]. One of the potential benefits of PET/MR compared with other imaging modalities may be improved detection and characterization of bone metastases.

Whole-body MR imaging has been shown to have superior diagnostic accuracy compared with CT and bone scintigraphy in detection of bone metastases because of its ability to assess early infiltration of bone marrow that precedes osteoblastic and osteoclastic response of the bone matrix to malignant tissue infiltration [4,2,5–7]. The comparison of whole-body MR and PET/CT for the detection of bone metastases in solid tumours and haematological malignancies yielded heterogeneous results depending on the tumour histology and the PET tracer used [8–14]. Importantly, integrated PET/CT has been reported to show a high positive predictive value of 98% for identification of bone metastases when both PET and CT components of the examination are concordant [15]. However, when CT and PET results are discordant, the positive predictive value of PET/CT significantly decreases to 61% [15]. The implementation of hybrid PET/MR imaging may potentially improve detection of early bone marrow infiltration, reduce the number of discordant findings and therefore increase diagnostic confidence in the detection and evaluation of bone metastasis.

It is not yet clear whether PET/MR provides a clinical benefit compared with PET/CT for the detection and evaluation of bone metastasis.

The aim of our study was to compare detection, lesion conspicuity and reader confidence of ^{18}F-FDG-PET/MR

0143-3636 DOI: 10.1097/MNM.0000000000000387

and ^{18}F-FDG-PET/CT in patients with ^{18}F-FDG avid bone metastases.

Materials and methods

Patients

In this prospective study, 24 patients (nine men, 15 women; median age 61.5 years, range 43–89 years) underwent sequential whole-body trimodality ^{18}F-FDG-PET/CT – MR between May 2011 and June 2013 as a part of clinical work-up for either staging or restaging/follow-up of various malignant tumours and suspicion of bone metastases (30 examinations). The primary diseases were breast cancer (12 patients), lung cancer (three patients), tonsil cancer (two patients), non-Hodgkin lymphoma (two patients) and carcinoma of the urethra, gastric cancer, cervical cancer, spindle cell skin cancer and medullary thyroid carcinoma (one patient each). Clinical indication for the PET/CT-examination was therapy follow-up (11 exams), primary staging (10 exams) and restaging (nine exams). All patients had histological confirmation of their primary disease. The mean follow-up period was 18.5 months (range: 12–36 months). No further selection was applied for patient inclusion. Patients unwilling to undergo an additional MR examination, those who had claustrophobia and those with MR-incompatible medical devices (e.g. cardiac pacemaker, insulin pump, neurostimulator, cochlear implant) were not considered for study inclusion. Six out of 24 patients underwent the PET/CT + MR study twice (mean interval 311 days) and, therefore, 30 studies were available for overall analysis. This study was approved by the institutional ethics committee and written informed consent was obtained from all patients before the examination. Patient characteristics are summarized in Table 1.

Table 1 Patient characteristics

Patient number	Age (years)	Sex	Diagnosis
1	46	F	Breast carcinoma
2	89	F	Breast carcinoma
3	54	F	Breast carcinoma
4	50	F	Breast carcinoma
5	44	F	Breast carcinoma
6	61	M	Renal carcinoma. Tonsil carcinoma
7	48	M	Malignant lymphoma
8	58	M	Spindle cell skin cancer
9	69	M	Medullary thyroid carcinoma
10	49	F	Breast carcinoma
11	81	F	Cancer of the uterine cervix
12	83	F	Breast carcinoma
13	44	F	Adenocarcinoma of the stomach
14	43	F	Lung adenocarcinoma
15	62	F	Breast carcinoma
16	69	M	Lung adenocarcinoma
17	66	F	Breast carcinoma
18	63	M	Malignant lymphoma
19	69	M	Lung adenocarcinoma
20	64	M	Carcinoma of the urethra
21	49	F	Breast carcinoma
22	78	F	Breast carcinoma
23	67	M	Tonsil carcinoma
24	58	F	Breast carcinoma

F, female; M, male.

Image acquisition

Sequential PET/CT and MR imaging was performed on a trimodality PET/CT-MR set-up (full-ring, time-of-flight Discovery PET/CT 690 and a 3-T Discovery MR 750; both GE Healthcare, Waukesha, Wisconsin, USA). Patients fasted for at least 4 h before injection of a standard dose of an average of 4.5 MBq /kg body weight of ^{18}F-FDG.

After injection, all patients were positioned on a dedicated shuttle board that was placed on top of the MR table. Patients had a resting time of ~30 min before going into the MR. A mechanism able to transfer the shuttle board from the MR-table to the PET/CT table ensured that patient transport from the MR system to the PET/CT and placement/removal of dedicated radiofrequency coils were possible without repositioning the patient [16]. With this, image sets of PET/CT and PET/MR were available for diagnostic and comparative purposes. After placing the patient onto the shuttle board, a dedicated radiofrequency coil (GEM 32-channel torso coil, posterior and anterior array combined; GE Healthcare) was positioned on the patient. The MR imaging protocol consisted of three different sequences. Whole-body multisection imaging was performed using a T1-weighted three-dimensional (3D) dual-echo gradient-recalled echo pulse sequence [liver accelerated volume acquisition (LAVA)-Flex; GE Healthcare]. LAVA acquisition was performed during end-expiratory breath-hold for breathing sensitive areas (thorax, abdomen). Whole-body multisection imaging was also performed with a coronally acquired short TI inversion recovery (STIR) sequence using parallel imaging. No breath-hold technique was used. Finally, a T2-weighted sequence with motion correction [periodically rotated overlapping parallel lines with enhanced reconstruction (Propeller); GE Healthcare] was acquired using a breathing trigger in the thorax. This sequence was used for enhanced breathing-triggered lung imaging. The total MR acquisition time was ca. 16 min. Detailed acquisition parameters for all MR sequences are presented in Table 2.

After completion of the MR examination, patients were shuttled to the PET/CT.

Low-dose CT data were acquired for PET attenuation correction (AC) and for diagnostic purposes. Tube voltage was 120 kV (peak), reference tube current was 12.35 mA/slice, automated dose modulation range was 15–80 mAs/slice, collimation was 64×0.625 mm, pitch was 0.984 : 1, rotation time was 0.5 s, field of view (FOV) was 50 cm and noise index was 20%. CT image sets were reconstructed using an iterative algorithm (Adaptive Statistical Iterative Reconstruction; GE Healthcare). The PET data were acquired in 3D TOF mode with a scan duration of 2 min per bed position, an overlap of bed

Table 2 Acquisition parameters for MR imaging

Parameters	LAVA	STIR	Propeller
TR/TE (ms)	4.3/1.3 (OP), 2.6 (IP)	2000/42	9321/122
Flip angle	12°	N/A	N/A
Partial Fourier	0.9%	N/A	N/A
TI (ms)	N/A	160	N/A
Partial imaging acceleration factor	2	2	3
Slice thickness (mm)	4.0	6	4.5
FOV (cm)	50	50	40
Acquisition matrix (pixels)	288×224	384×224	288×288
Receiver bandwidth (kHz)	142.86	100	62.5
Acquisition time per body section (s)	18	123	N/A
Body sections per patient	4	3	1
Total acquisition time (min)	ca. 3	ca. 8	ca. 5
Coverage	Whole body	Whole body	Chest, upper abdomen

FOV, field of view; IP, in-phase; LAVA, liver accelerated volume acquisition, T1-weighted 3D dual-echo gradient-recalled echo pulse sequence; OP, opposed phase; Propeller, periodically rotated overlapping parallel lines with enhanced reconstruction, T2-weighted sequence with motion correction; STIR, short TI inversion recovery sequence; TE, time to echo; TI, inversion time; TR, time of repetition.

positions of 23%, an axial FOV of 153 mm and a 700 mm diameter FOV. The emission data were corrected for attenuation using the low-dose CT (CTAC) and iteratively reconstructed [matrix size 256×256, VUE Point FX (3D TOF-OSEM) with three iterations, 18 subsets]. Images were filtered in image space using an in-plane Gaussian convolution kernel with a full-width at half-maximum of 4.0 mm, followed by a standard axial filter with a three-slice kernel. This procedure has been used in this standard manner in other studies as well [17].

Image processing

The PET, CT and MR images acquired were sent to a dedicated review workstation (Advantage workstation, version 4.6; GE Healthcare) that enables simultaneous review of PET, CT and MR images side by side or in fused/overlay mode (PET/CT, PET/MR). For this study, PET/CT and PET/MRI data sets were compared. The standard of reference consisted of histology (if available) or follow-up with at least one additional cross-sectional imaging examination.

Image analysis

Assessment of lesions in all below-mentioned categories was performed by two readers (certified in radiology and nuclear medicine) in consensus. PET/CT was evaluated first. Then, with a time gap of 6 weeks, the PET/MR images were also evaluated by the same readers in consensus. The readers were blinded to any possible previous PET/CT or MR imaging. However, the readers were aware of the diagnosis of the patients and were aware of the clinical question for the respective clinical PET/CT.

Detection of PET-positive bone lesions

First, each PET examination was evaluated for the presence of PET-positive bone lesions. Lesions were considered PET positive if their maximum standardized uptake value (SUV_{max}) was significantly higher than liver uptake. In cases where increased uptake was visible but inferior to liver uptake, the surrounding tissue was taken as a reference. For every lesion SUV_{max}, the mean standardized uptake value (SUV_{mean}), total lesion glycolysis and metabolic tumour volume (PET_{vol}) were measured. The threshold value as percentage of SUV_{max} was adjusted manually for each lesion such that the borders of the volume of interest only included activity that could be ascribed to the lesion. The location and the number of the lesions were recorded. Up to ten PET-positive lesions were evaluated per patient with a maximum of three lesions per body compartment (e.g. cervical, thoracic, lumbar spine, pelvis). In patients with multiple confluent lesions in the same compartment, lesions that were clearly distinguishable from each other were selected for analysis. ^{18}F-FDG-negative lesions with benign radiological appearance were not evaluated in this study.

Lesion conspicuity

The conspicuity of PET-positive bone lesions was evaluated on the corresponding PET/CT and PET/MR images. For this analysis, the conspicuity of the morphological imaging component was assessed (CT or MR). Lesions were assessed on the basis of a five-point scale: grade 0 – lesion was not detectable, grade 1 – 1–25% lesion contour detectable, grade 2 – 26–50% contour detectable, grade 3 – 51–75% contour detectable and grade 4 – 76–100% contour detectable. The evaluation described was applied for all the reconstructions of the T1-weighted 3D gradient echo sequence (in-phase, out-phase, fat and water), for the whole-body STIR sequence and for the CT images. A time gap of 6 weeks between the assessment of PET/CT and PET/MR images was applied to eliminate potential bias.

Lesion size

Measurements of the maximum lesion diameters on CT and MR images were obtained. Lesions not visible on the CT or MR images were not measured in that particular modality and noted as 'not measurable'. Measurements on the MRI component were taken on the reconstructed T1 in-phase images.

Lesion density

All lesions were assigned to three groups on the basis of their CT appearance. (a) Sclerotic lesions with predominantly an increase in bone density. (b) Lytic lesions with predominantly destruction of bone tissue. (c) ^{18}F-FDG-positive lesions without change in bone density, for example lesions not visible on CT imaging.

Reader confidence

Reader confidence was determined qualitatively to evaluate whether PET/CT or PET/MR was more useful for the assessment of the evaluated bone metastases. The following score was used for assessment.

High reader confidence

^{18}F-FDG-positive lesions had a morphologic correlate and overall hybrid imaging findings correlated to metastatic involvement – 2 points.

Moderate reader confidence

PET-positive findings are suggestive of metastatic disease, but only partially show a morphologic correlate – 1 point.

Low reader confidence

PET findings are inconclusive, no clear morphologic correlate is seen for ^{18}F-FDG-positive lesions – 0 points.

Statistical analysis

Ordinal variables were expressed as median (range), nominal variables as mode (percentage) and ratio variables as geometric mean ± SD. For the purpose of clarity, the conspicuity score was also expressed as mean ± SD. The size and conspicuity of lesions in different modalities were compared using the Wilcoxon signed-ranks test for matched pairs. Size, conspicuity and PET parameters of lesions stratified by CT-density and location on CT and MR images were compared using the Mann–Whitney *U*-test for independent samples. Reader confidence was compared using Student's *t*-test. A *P*-value of less than 0.05 was considered statistically significant. All statistical analyses were carried out with IBM SPSS Statistics 19.0.1 (IBM, Armonk, New York, USA).

Results

A total of 30 PET/CT and PET/MRI data sets were performed in 24 patients. A total of 86 ^{18}F-FDG-positive bone lesions were identified. In 12 data sets, patients had multiple disseminated bone lesions, whereas in the remaining 18 data sets, less than 10 lesions were present in each patient. The metabolic and morphologic characteristics of the lesions are summarized in Table 3.

Table 3 Summary of metabolic and morphologic characteristics of all ^{18}F-FDG-positive bone lesions

	N	Minimum	Maximum	Mean	SD
Metabolic characteristics					
SUV_{max}	86	2.2	29.7	7.96	5.2
SUV_{mean}	86	1.2	14.2	4.6	2.69
TLG	86	477	441 931	32 243.91	77 688.86
PET_{vol}	86	0.42	83.8	5.74	12.1
Size (mm)					
CT	65	4	84	17.03	16.77
MR T1 in-phase	82	5	85	20.63	17.2
Conspicuity, score					
CT	86	0	4	2.35	1.62
MR STIR	86	0	4	2.23	1.57
MR T1 water	86	0	4	2.48	1.42
MR T1 fat	86	0	4	3.09	1.44
MR T1 in-phase	86	0	4	2.21	1.46
MR T1 out-phase	86	0	4	2.76	1.47

MR T1 water, fat, in-phase, out-phase, T1-weighted 3D dual-echo gradient-recalled echo pulse sequence, liver accelerated volume acquisition, corresponding water, fat, in-phase and out-phase reconstruction; MR STIR: short TI inversion recovery sequence; PET_{vol}, metabolic tumour volume; SUV_{max}, maximum standardized uptake value; SUV_{mean}, mean standardized uptake value; TLG, total lesion glycolysis.

Detection

Overall, in both examinations, PET/CT and PET/MRI detected the same number of lesions on the basis of the PET component (as both examinations used the same PET-data set).

In those 30 data sets, 95% of analyzed ^{18}F-FDG-positive bone lesions (82/86 lesions) had a morphologic correlate on the MR component. Thus, on all PET/MRI examinations, at least one morphological correlate was found on the MR component.

PET/CT imaging enabled identification of structural changes on the CT component in 76% of the ^{18}F-FDG-positive lesions (65/86 lesions). A morphologic correlate on the CT component of the PET/CT was clearly identified in 23 PET/CT studies out of 30.

Overall, in seven examinations (seven patients), ^{18}F-FDG-positive bone lesions ($n = 9$) were seen only on the MR component without clearly visible changes of the bony structure on CT. In two of these examinations (two patients), patients had one single ^{18}F-FDG-positive lesion that was not visible on MR or CT images. However, in both of these examinations, a single additional ^{18}F-FDG-positive bone lesion (two lesions in total) was seen again only on the MR component in a different location. No additional lesions were seen on the CT component in those cases. The remaining lesions that were ^{18}F-FDG positive but CT negative were all seen in patients where several other bone metastases were detected on both the PET component and the CT component.

In two different examinations (two patients), the structural bone change in two ^{18}F-FDG-positive lesions was seen only in the CT component but not in the MRI component. Again, in those patients, additional ^{18}F-FDG-positive bone lesions (four lesions) showed a morphological correlate on the MR component.

Reader confidence

The overall reader confidence on the basis of the abovementioned scale for PET/CT was 1.76 and 2.0 for PET/MRI ($P = 0.0029$). PET/MR showed a high confidence in all patients. However, in PET/CT, a high confidence was found in 23 cases and a moderate confidence in seven cases (Figs 1 and 2). In 23 studies, no change in reader confidence was observed between PET/CT and PET/

Fig. 1

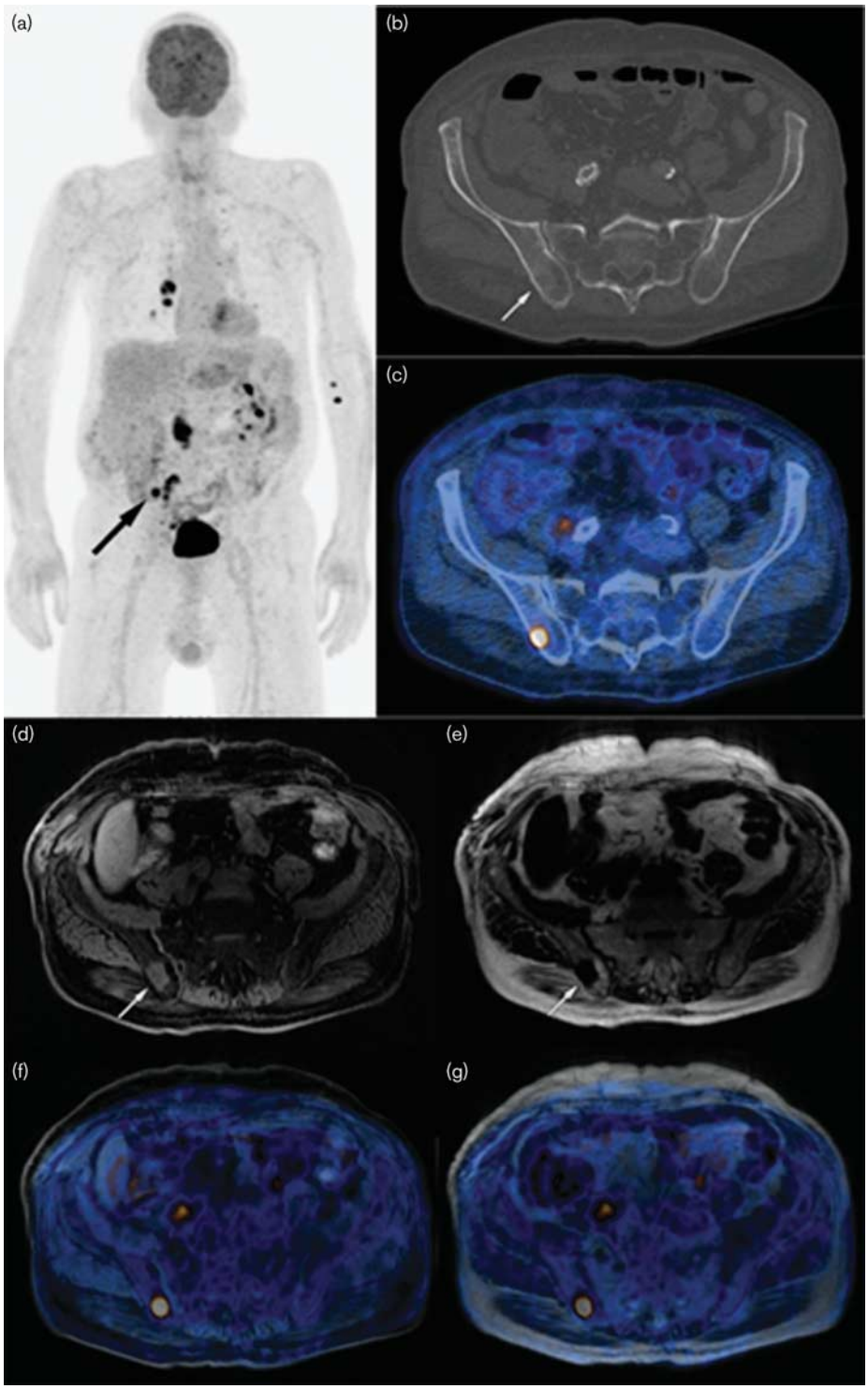

Male patient (64 years old) with metastatic carcinoma of the urethra. (a) Three-dimensional ^{18}F-FDG-PET image shows metastatic spread of the cancer. A single ^{18}F-FDG avid bone metastasis is present in the right iliac bone (black arrow). (b) On axial CT image, only the partially visible sclerotic lesion is seen in the corresponding location (white arrow) – such findings can be easily overseen when reading CT images prospectively. (c) Fused PET/CT axial image. (d, e) In contrast to the CT image, this single bone lesion is clearly depicted on axial MR images (white arrows) as a signal increase on the T1 water image (d) and as a signal drop on the T1 fat image (e) compared with the normal bone marrow. (f, g) Corresponding fused PET/MR images. In this case, PET/MR imaging provided higher reader confidence for the diagnosis of metastatic bone marrow involvement compared with the PET/CT imaging as a morphologic correlate for the ^{18}F-FDG avid bone lesion was clearly seen only on MR imaging. CT, computed tomography; ^{18}F-FDG, ^{18}F-fluorodeoxyglucose.

Fig. 2

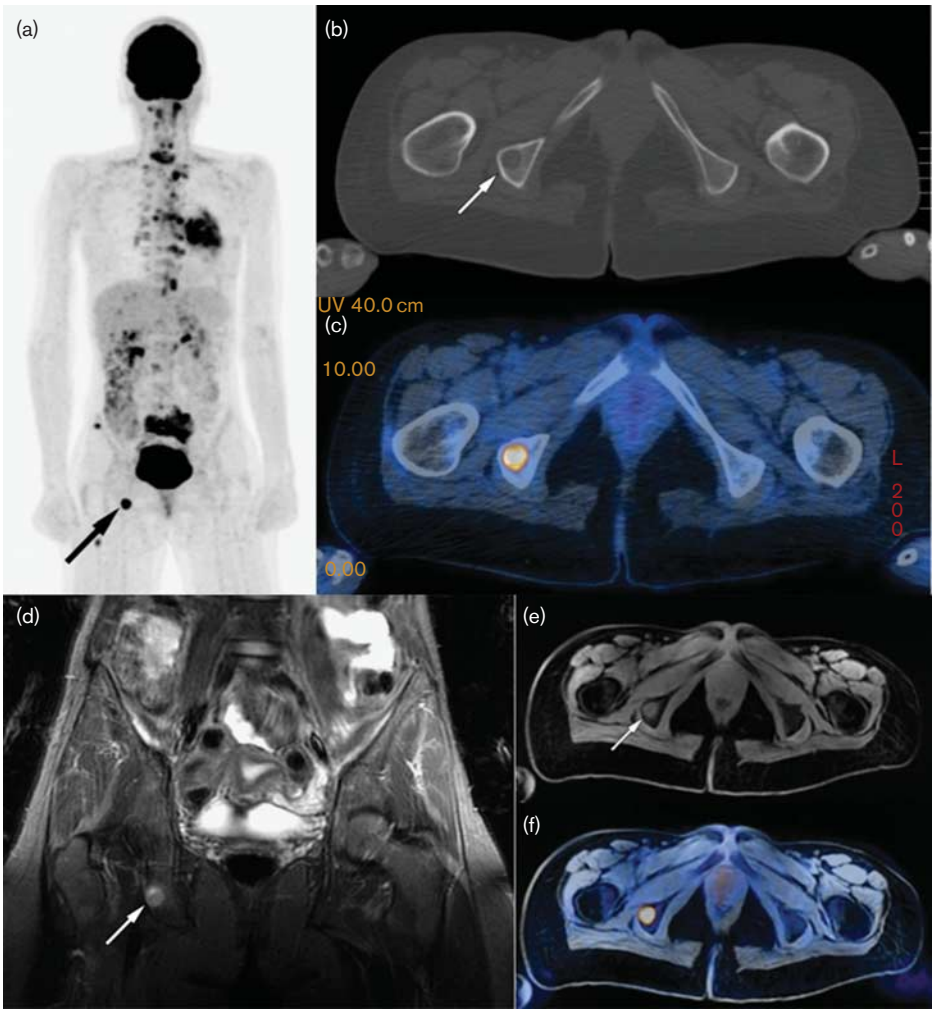

Female patient (43 years old) with adenocarcinoma of the lung. (a) Three-dimensional ^{18}F-FDG-PET image shows metastatic spread of the cancer. One of the multiple ^{18}F-FDG avid bone metastases is present in the right ischium (black arrow). (b) Axial CT image shows clear osteolysis in the corresponding location (white arrow). (c) Fused PET/CT axial image. (d) Coronal STIR MR image and (e) axial T1 water image clearly depict the lesion because of its high signal intensity (white arrows). (f) Corresponding axial fused PET/MR image. In this case, PET/CT and PET/MR imaging provided equal reader confidence for the diagnosis of metastatic bone marrow involvement as a morphologic correlate for the ^{18}F-FDG avid bone lesion was clearly seen on both CT and MR images. CT, computed tomography; ^{18}F-FDG, ^{18}F-fluorodeoxyglucose.

MR imaging. These patients either had several lesions seen on both modalities or had multiple disseminated lesions where the difference in the detection of single lesions did not lead to a change in overall reader confidence. Thus, in the seven studies in which all ^{18}F-FDG-positive bone lesions ($n = 9$) were seen only on the MR component, a significant increase was found in reader confidence for PET/MRI versus PET/CT.

Lesion conspicuity

In lesion-by-lesion analysis, PET/MR imaging provided better results in the detection of morphologic changes in the ^{18}F-FDG-positive bone lesions analysed: the mean lesion conspicuity was significantly better on T1 fat MR imaging compared with CT imaging ($P = 0.005$, Table 4). The overall lesion conspicuity on STIR-weighted MR images was similar to CT images.

Table 4 Comparison of lesions conspicuity scores between CT and MR images

Lesions' conspicuity	*P*-value
MR STIR vs. CT	0.496
MR T1 water vs. CT	0.516
MR T1 fat vs. CT	0.005[a]
MR T1 in-phase vs. CT	0.834
MR T1 out-phase vs. CT	0.069

CT, computed tomography; MR T1 water, fat, in-phase, out-phase, T1-weighted 3D dual-echo gradient-recalled echo pulse sequence, liver accelerated volume acquisition, corresponding water, fat, in-phase and out-phase reconstruction; MR STIR: short TI inversion recovery sequence.
[a]The mean lesion conspicuity was significantly higher on T1 fat MR imaging compared with CT imaging.

Table 5 Conspicuity scores (mean values) of the lesions on the basis of their CT density

	Lytic	Sclerotic	Nonvisible on CT
N of lesions (CT based)	48	17	21
CT score	3.08	3.18	0
MR STIR score	2.11	1.88	2.88
MR T1 water score	2.3	2.86	2.48
MR T1 fat score	2.77	3.37	3.52
MR T1 in-phase score	1.88	2.52	2.21
MR T1 out-phase score	2.53	3	3.05

CT, computed tomography; MR T1 water, fat, in-phase, out-phase, T1-weighted 3D dual-echo gradient-recalled echo pulse sequence, liver accelerated volume acquisition, corresponding water, fat, in-phase and out-phase reconstruction; MR STIR: short TI inversion recovery sequence.

In the subanalysis based on lesions density (on the CT-component), the mean conspicuity of neither lytic nor sclerotic lesions was significantly different on T1 fat MR imaging compared with CT imaging. However, the mean conspicuity of both sclerotic and lytic lesions was significantly higher on CT imaging compared with STIR MR imaging ($P = 0.014$ and 0.004, respectively). Further characteristics of this subanalysis are summarized in Tables 5 and 6.

In the 21 ^{18}F-FDG-positive bone lesions without a corresponding structural change visible in PET/CT imaging (65/86 were seen), the lesions were seen best in the T1 fat sequence of PET/MR imaging with a mean conspicuity of 3.52 and a mean size on T1 imaging of 19.5 mm. Further characteristics of these lesions are summarized in Table 7. The mean size of the ^{18}F-FDG-positive bone lesions was found to be significantly larger on T1-weighted MR images compared with CT images.

Discussion

In our study, we found that the overall detection rate of PET/CT and PET/MRI was the same on the basis of the ^{18}F-FDG positivity of the bone metastases evaluated here.

However, we could show that lesion conspicuity as well as reader confidence were improved in PET/MRI compared with PET/CT on the basis of the soft tissue contrast of the MR component. Furthermore, several morphological correlates were identified in PET/MRI that were not present in PET/CT.

Table 6 Comparison of sclerotic and lytic lesions conspicuity scores between CT and MR images

Lesions' conspicuity	*P*-value
Lytic lesions	
MR STIR vs. CT	0.004[a]
MR T1 fat vs. CT	0.309
Sclerotic lesions	
MR STIR vs. CT	0.014[b]
MR T1 fat vs. CT	0.425

CT, computed tomography; MR T1 water, fat, in-phase, out-phase, T1-weighted 3D dual-echo gradient-recalled echo pulse sequence, liver accelerated volume acquisition, corresponding water, fat, in-phase and out-phase reconstruction; MR STIR: short TI inversion recovery sequence.
[a,b]Mean conspicuity of both sclerotic and lytic lesions was significantly higher on CT imaging compared with STIR MR imaging.

Table 7 Metabolic and morphologic characteristics (mean values) of ^{18}F-FDG-positive bone lesions nonvisible on CT by location

	Thorax	Spine	Pelvis	Extremities	Total
N	2	7	6	6	21
Metabolic characteristics					
SUV_{max}	4.6	7.4	17.6	7.8	10.1
SUV_{mean}	2.2	4.3	8.3	4.9	5.4
Size (mm)					
MR T1 in-phase	17	18.3	28.5	13.7	19.5
Conspicuity, score					
MR STIR	1	2.3	3.7	3.7	2.9
MR T1 water	1	3.1	3.3	2.7	2.9
MR T1 fat	1	3.9	3	3.3	3.5
MR T1 in-phase	1	2.9	3	2.2	2.5
MR T1 out-phase	1	3.3	3.7	2.8	3.1

CT, computed tomography; ^{18}F-FDG, ^{18}F-fluorodeoxyglucose; MR T1 water, fat, in-phase, out-phase, T1-weighted 3D dual-echo gradient-recalled echo pulse sequence, liver accelerated volume acquisition, corresponding water, fat, in-phase and out-phase reconstruction; MR STIR: short TI inversion recovery sequence; SUV_{max}, maximum standardized uptake value; SUV_{mean}, mean standardized uptake value.

General

The superior soft tissue contrast and the consecutive ability to assess early metastatic infiltration of bone marrow make PET/MRI a promising modality in staging and response assessment in metastatic bony disease compared with PET/CT. However, compared with PET/CT as a standard of reference, PET/MRI as a new technology should have clear advantages in patient care and should ideally not place additional examination burden on the patients. There is a general workflow issue currently discussed in the literature with current PET/MRI protocols. Most of the protocols in such an early phase of a new modality are just 'normal' MR protocols that do not take into account the additional diagnostic information of the PET component. However, in our study, here, we evaluated a PET/MRI protocol that consists of three noncontrast sequences that allow for a whole-body PET/MRI approximately within the same time than a standard PET/CT [17].

Current literature

Our study suggests that one of the clinical scenarios where PET/MRI may be beneficial over PET/CT is an oncological patient with only few early bone metastases. In our series of patients, 25% of the lesions evaluated showed no definite morphological change in the bony structure on CT imaging whereas 95% of lesions had a clear morphological correlate on MR imaging. Although all these lesions were still detected because of their ^{18}F-FDG avidity, in cases of low metabolic activity (e.g. post-therapy), moving artefacts and small size, a pathological ^{18}F-FDG uptake in those lesions might not be very obvious. In this situation, the clear depiction of lesions on the MR component would ensure the detection of the lesions and correct distant staging of the

disease. This observation is supported by the recent work of Eiber *et al.* [18], who drew a similar conclusion .

The presence of ^{18}F-FDG-positive bone lesions on PET with negative findings at CT is not uncommon and is a known clinical issue. In the study by Taira *et al.* [15], 27% (31 out of 113) of ^{18}F-FDG-positive bone lesions analysed were found to be CT negative. In addition, MRI has been shown to find metastasis not visible on ^{18}F-FDG-PET or CT imaging [9]. In an early comparison, Antoch *et al.* [8] reported that MRI was more accurate in evaluating the bone structure for the presence of metastasis in a study comparing the staging accuracies of whole-body MRI and PET/CT. These finding were later supported in a study by Schmidt *et al.* [12], where whole-body MR imaging was found to have superior sensitivity and accuracy compared with PET/CT in the detection of bone metastases [12]. Therefore, in PET/MRI, even in cases of low ^{18}F-FDG activity, the likelihood of correct detection and staging seems to be higher than PET/CT. However, according to the results of our study, in patients with a high likelihood of metastatic bone disease, the use of PET/MRI would likely not result in improved diagnostic confidence as both PET/CT and PET/MRI would detect multiple lesions with no further therapeutic consequence.

Overall, we found an improved lesion conspicuity as well as higher reader confidence in the evaluation of PET/MRI compared with PET/CT. The lesion-by-lesion analysis showed that the highest lesion conspicuity was achieved by PET/MR imaging using the T1-weighted sequence highlighting the alterations in the bone marrow (T1 fat reconstruction). The significant increase in lesions conspicuity on MR imaging was mainly because of 21 ^{18}F-FDG-positive bone lesions not visible on CT imaging. These lesions likely represent bone marrow infiltration that have not yet resulted in considerable change in bone density but already changed signal in MR imaging [1]. Interestingly, the mean size of these lesions was quite substantial (19.5 mm). These results are partly in agreement with a recent study with a similar number of evaluated lesions [18]. There, PET/MRI with a T1-weighted sequence in addition to the Dixon-based AC sequence was superior in lesion delineation. Several differences have to be noted compared with our study. One of the reasons for the improved delineation in this additional T1-weighted sequence might be the higher matrix compared with the Dixon sequence. However, overall detection was not significantly different. Additional differences are that the PET/CT was partly performed with contrast media compared with a non-contrast PET/MRI. In our study, we strictly used non-contrast PET/CT for our comparison. An important aspect that was evaluated in our study was the reader confidence. Interestingly, although overall lesion detection was the same between PET/CT and PET/MRI, the additionally detectable lesions on the MRI component obviously support the diagnostic confidence for the reader – a fact that cannot be neglected in clinical routine reading, again, especially in lesions with low ^{18}F-FDG uptake.

Several studies have evaluated the important issue of differences in AC in PET imaging deriving from CT-based AC or MR-based AC. Phantom studies showed an increase in the relative error by up to 6.8% in the body and up to 31.0% for bony regions when the bones are ignored by the AC algorithm. In simulated clinical studies, the mean relative error may be as high 15% for body lesions and 30.7% for bony lesions [19]. Differences for the head and brain are lower [20]. These issues certainly have an impact on the detection of metastatic bone disease in simultaneous PET/MRI. These issues are even more pronounced when simulating therapy response, where it was found that simulated PET AC leads to a considerable underestimation of tracer uptake in bone lesions. The underestimation is dependent on the lesion composition with the largest error in sclerotic lesions [21]. As we used a trimodality set-up for our evaluation, we cannot compare or comment on those differences; however, this might be considered an advantage of the trimodality set-up for scientific comparisons where no underestimation can occur. Interestingly, in our patient population, the mean conspicuity of neither lytic nor sclerotic lesions was significantly different on T1 imaging compared with CT density. However, there was a difference in sclerotic and lytic lesions compared with STIR. This is remarkable, because usually – in MR imaging – fat-saturated T2 imaging is considered the ideal sequence to search for the major pathologies and especially bone lesions [22,23]. In PET/MRI (or PET/CT-MRI), the PET component is always available (no choice), but one has a choice which sequences are being used in the MR part of the examination. Thus, in the context of PET/MR, the sequences of choice might be different from those in MR imaging alone.

Limitation

The possible limitation of the study is that only ^{18}F-FDG-positive bone lesions were selected for the analysis. Thus, evaluation of benign lesions is not part of this study. Histological verification of ^{18}F-FDG-positive bone lesions was not always possible (and ethically not justifiable), but all patients had histological verification of their primary disease and the available imaging and clinical data were used to assess the analysed lesions on the basis of standard imaging criteria. We did not evaluate a possible clinical impact of PET/MR versus PET/CT in our patient population.

Conclusion

PET/MRI offers higher diagnostic confidence and an improved conspicuity in bone metastases compared with PET/CT. However, the overall detection rate was not

different. The highest possible clinical impact of PET/MRI appears to be in patients with limited early bone metastatic disease.

Acknowledgements

This research project was supported by an institutional research grant from GE Healthcare. Research by Andrei Samarin was supported by the European Union through the European Regional Development Fund.

Conflicts of interest

Patrick Veit-Haibach received IIS Grants from Bayer Healthcare, Siemens Medical Solutions, Roche Pharmaceutical and speaker fees from GE Healthcare. Gustav von Schulthess is a grant recipient from GE Healthcare and receives speaker fees from GE Healthcare. For the remaining authors there are no conflicts of interest.

References

1 Choi J, Raghavan M. Diagnostic imaging and image-guided therapy of skeletal metastases. *Cancer Control* 2012; **19**:102–112.
2 Lecouvet FE, Larbi A, Pasoglou V, Omoumi P, Tombal B, Michoux N, *et al.* MRI for response assessment in metastatic bone disease. *Eur Radiol* 2013; **23**:1986–1997.
3 Pace L, Nicolai E, Aiello M, Catalano O, Salvatore M. Whole-body PET/MRI in oncology: current status and clinical applications. *Clin Transl Imaging* 2013; **1**:31–44.
4 Engelhard K, Hollenbach HP, Wohlfart K, von Imhoff E, Fellner FA. Comparison of whole-body MRI with automatic moving table technique and bone scintigraphy for screening for bone metastases in patients with breast cancer. *Eur Radiol* 2004; **14**:99–105.
5 Mentzel HJ, Kentouche K, Sauner D, Fleischmann C, Vogt S, Gottschild D, *et al.* Comparison of whole-body STIR-MRI and ^{99m}Tc-methylene-diphosphonate scintigraphy in children with suspected multifocal bone lesions. *Eur Radiol* 2004; **14**:2297–2302.
6 Steinborn MM, Heuck AF, Tiling R, Bruegel M, Gauger L, Reiser MF. Whole-body bone marrow MRI in patients with metastatic disease to the skeletal system. *J Comput Assist Tomogr* 1999; **23**:123–129.
7 Yang HL, Liu T, Wang XM, Xu Y, Deng SM. Diagnosis of bone metastases: a meta-analysis comparing (1)(8)FDG PET, CT, MRI and bone scintigraphy. *Eur Radiol* 2011; **21**:2604–2617.
8 Antoch G, Vogt FM, Freudenberg LS, Nazaradeh F, Goehde SC, Barkhausen J, *et al.* Whole-body dual-modality PET/CT and whole-body MRI for tumor staging in oncology. *JAMA* 2003; **290**:3199–3206.
9 Ghanem NA, Pache G, Lohrmann C, Brink I, Bley T, Kotter E, *et al.* MRI and (18)FDG-PET in the assessment of bone marrow infiltration of the spine in cancer patients. *Eur Spine J* 2007; **16**:1907–1912.
10 Heusner T, Golitz P, Hamami M, Eberhardt W, Esser S, Forsting M, *et al.* "One-stop-shop" staging: should we prefer FDG-PET/CT or MRI for the detection of bone metastases? *Eur J Radiol* 2011; **78**:430–435.
11 Qu X, Huang X, Yan W, Wu L, Dai K. A meta-analysis of (1)(8)FDG-PET-CT, (1)(8)FDG-PET, MRI and bone scintigraphy for diagnosis of bone metastases in patients with lung cancer. *Eur J Radiol* 2012; **81**:1007–1015.
12 Schmidt GP, Schoenberg SO, Schmid R, Stahl R, Tiling R, Becker CR, *et al.* Screening for bone metastases: whole-body MRI using a 32-channel system versus dual-modality PET-CT. *Eur Radiol* 2007; **17**:939–949.
13 Wu LM, Chen FY, Jiang XX, Gu HY, Yin Y, Xu JR. ^{18}F-FDG PET, combined FDG-PET/CT and MRI for evaluation of bone marrow infiltration in staging of lymphoma: a systematic review and meta-analysis. *Eur J Radiol* 2012; **81**:303–311.
14 Zamagni E, Nanni C, Patriarca F, Englaro E, Castellucci P, Geatti O, *et al.* A prospective comparison of ^{18}F-fluorodeoxyglucose positron emission tomography-computed tomography, magnetic resonance imaging and whole-body planar radiographs in the assessment of bone disease in newly diagnosed multiple myeloma. *Haematologica* 2007; **92**:50–55.
15 Taira AV, Herfkens RJ, Gambhir SS, Quon A. Detection of bone metastases: assessment of integrated FDG PET/CT imaging. *Radiology* 2007; **243**:204–211.
16 Kuhn FP, Crook DW, Mader CE, Appenzeller P, von Schulthess GK, Schmid DT. Discrimination and anatomical mapping of PET-positive lesions: comparison of CT attenuation-corrected PET images with coregistered MR and CT images in the abdomen. *Eur J Nucl Med Mol Imaging* 2013; **40**:44–51.
17 Huellner MW, Appenzeller P, Kuhn FP, Husmann L, Pietsch CM, Burger IA, *et al.* Whole-body nonenhanced PET/MR versus PET/CT in the staging and restaging of cancers: preliminary observations. *Radiology* 2014; **273**:859–869.
18 Eiber M, Takei T, Souvatzoglou M, Mayerhoefer ME, F yer S, Gaertner FC, *et al.* Performance of whole-body integrated 18F-FDG PET/MR in comparison to PET/CT for evaluation of malignant bone lesions. *J Nucl Med* 2014; **55**:191–197.
19 Akbarzadeh A, Ay MR, Ahmadian A, Alam NR, Zaidi H. MRI-guided attenuation correction in whole-body PET/MR: assessment of the effect of bone attenuation. *Ann Nucl Med* 2013; **27**:152–162.
20 Larsson A, Johansson A, Axelsson J, Nyholm T, Asklund T, Riklund K, Karlsson M. Evaluation of an attenuation correction method for PET/MR imaging of the head based on substitute CT images. *MAGMA* 2013; **26**:127–136.
21 Samarin A, Burger C, Wollenweber SD, Crook DW, Burger IA, Schmid DT, *et al.* PET/MR imaging of bone lesions – implications for PET quantification from imperfect attenuation correction. *Eur J Nucl Med Mol Imaging* 2012; **39**:1154–1160.
22 Vanel D, Casadei R, Alberghini M, Razgallah M, Busacca M, Albisinni U. MR imaging of bone metastases and choice of sequence: spin echo, in-phase gradient echo, diffusion, and contrast medium. *Semin Musculoskelet Radiol* 2009; **13**:97–103.
23 Vanel D, Dromain C, Tardivon A. MRI of bone marrow disorders. *Eur Radiol* 2000; **10**:224–229.